J. Shanghai Jiaotong Univ. (Sci.), 2011, 16(1): 55-60
DOI: 10.1007/s12204-011-1094-7

Multi-element Ultrasound Phased Array Applicator for the Ablation of Deep-seated Tissue

JI Xiang (吉　翔), *SHEN Guo-feng** (沈国峰), *BAI Jing-feng* (白景峰), *LI De-hui* (李德辉)
YU Ying (余　瑛), *QIAO Shan* (乔　杉), *CHEN Ya-zhu* (陈亚珠)
(Biomedical Instrument Institute, Med-X Research Institute, Shanghai Jiaotong University, Shanghai 200030, China)

© Shanghai Jiaotong University and Springer-Verlag Berlin Heidelberg 2011

Abstract: High-intensity focused ultrasound (HIFU) has attracted increasing interests as a promising noninvasive modality for the treatment of deep tumors in the thoracic and abdominal cavity. A 90-element HIFU spherical phased array applicator operated at 1 MHz has been developed for deep tissue ablation. The spherical array with a 5 cm wide central hole has a 21 cm diameter and an 18 cm radius of curvature. Annular element distribution with unequal element spacing is used to reduce the number of elements. The array is constructed with piezoelectric lead zirconate titanate (PZT-8) circular elements that are 1.4 cm in diameter and have a wall with thickness of 0.2 cm. The array offers an effective ablating depth of at least 8 cm in the tissue for both simulations and ex vivo experiments. The simulations demonstrate that the developed array can steer the focus with good quality of intensity distributions up to 6 mm off center over ranges from 17 to 21 cm when the water depth is set at 11 cm. We also present the beam focusing capability in deep tissue through a series of ex vivo experiments by measuring discoloration areas after sonications. These results indicate that the developed array is ideal for the ablation of deep-seated tissue.
Key words: high-intensity focused ultrasound (HIFU), spherical phased array, focus pattern, ablation
CLC number: Q 62, Q 65　　**Document code:** A

0 Introduction

With great advances in medical imaging techniques, high-intensity focused ultrasound (HIFU), as a noninvasive therapy, has been used clinically in tumor treatments since 1990s[1]. Let M denote the number of element. Although single-element ($M = 1$) self-focused transducers and acoustic lens-focused transducers have demonstrated that they can ablate target volumes deep within the body in HIFU treatment, multiple-element ($M > 4$) phased-array transducers offer the advantages of electronic beam focusing and steering without mechanically moving the transducers. Thus, deep tissue ablation using HIFU transducer, especially phased arrays, may have greater potential in ablating deep solid tumors within the thoracic and abdominal cavity.

Spherical phased array has been widely used in HIFU because it can generate the beam focusing and steering with high intensity gain, small focal spot size, and low grating lobe level as a spot-scanning applicator for deep localized hyperthermia[2]. Previously many studies have been carried out on spherical phased arrays, including the guidelines in the spherical array design for desired focal volumes[3], sparse random phased array for focal surgery[4], pseudo inverse method for focus pattern synthesis[5], and the theoretical assessment of the performance of spherical phased arrays[6]. To date, several spherical phased array applicators with different shapes[7-9] have been designed and constructed for ablating deep-seated tissue. One example of these arrays is a 256-element array with equally sized element projections, and has generated lesions at depths of 2 to 5.5 cm underneath the skin through in vivo porcine experiments. Another experimental design is a 256-element toroidal array divided into 8 emitters, and the mean depth of the HIFU lesions generated by that array was over 2 cm in the ex vivo liver experiments[9]. These experimental results have shown the capability of the above phased arrays to ablate deep tissue. However, these applicators were comprised of over 200 elements with compact arrangements. The large number of elements did not only increase the cost and complexity of their supporting ultrasound driving system, but they also needed high transducer fabrication levels to get

Received date: 2010-04-23
Foundation item: the National Natural Science Foundation of China (No. 30800246), the Shanghai Key Technologies R&D Program of China (No. 09441500900) and the Med-X Shanghai Engineering Center Foundation (No. 08DZ2211201)
∗**E-mail:** shenguofeng@sjtu.edu.cn

each element cut into a small area. Therefore, it necessitates a trade-off between the target ablation volume and the cost in the array design. In this study, a spherical phased array for the ablation of deep-seated tissue is designed and constructed with a relatively small number of elements ($M < 100$) but larger scale geometry.

The objective of this study is to design, construct, and test a large-scale spherical ultrasound phased array with a relatively small number of elements ($M < 100$) for the ablation of deep tissue (effective focal depth $d > 10$ cm). To accomplish this goal, a large-scale spherical geometry was first chosen for this array, while unequal inter-element spacing was used to reduce the number of elements. The designed array was then constructed using 90 PZT-8 elements. The pseudo inverse method combined with the ultrasound field calculation in a water-muscle medium was used in simulations and experiments. The capability to focus and steer beams at different depths of tissue was then tested for the developed array in the simulations. Finally, experiments in ex vivo porcine muscle were conducted to confirm the ability of this array for deep tissue ablation.

1 Materials and Methods

1.1 Array Design and Construction

A spherical-section phased array with large aperture has the ability to electronically focus and steer the beam in a 3D volume and generate multiple-focus patterns[2]. Therefore, a large-scale spherical geometry was first chosen in the array design. For this study, the array was designed to ablate the target volume at a focal depth of more than 10 cm and to consist of less than 100 elements. Taking into account the required effective focal depth ($d > 10$ cm) and the practical possible maximum ablation depth, an 18 cm radius of curvature was then set for the array. The array f number should be less than 1.0 to minimize the near field heating[10]. In addition, in order to control the number of elements ($M < 100$) the diameter of the array was chosen to be 21 cm (f =0.86). The resonance frequency of elements was set at 1.0 MHz to avoid the cavitation caused by low frequency ultrasound and the increased attenuation of high frequency ultrasound. Compared with the compact arrangements of elements in Refs. [7,9], the designed array offered an element distribution wherein the elements were distributed in an annular shape, and each ring arranged the same number of elements. All angles (θ_o) between the elements in the odd rings and x-axis were equal, which were uneven with the counterparts (θ_e) in the even rings. In short, $\theta_o \neq \theta_e$ (see Fig. 1(b)). Unequal inter-element spacing was also used to reduce the element number wherein the inter-element spacings in every two neighboring rings varied. In addition, the vertical distances between two neighboring rings also varied. The element size was then determined by maximizing the surface area of the array under the circumstance of the element number less than 100. The array parameters (element size and element number) were simulated to ensure that the array could steer the single focus within the target volume (a $\pi \times 1.0 \times 1.0$ cm^2 area in the focal plane) without generating the grating lobes more than 25% of the main lobe. Using these parameters, the designed array for this study contained an 18 cm radius of curvature and a 21 cm diameter with 90 identical circular elements 1.4 cm in diameter (see Fig. 1).

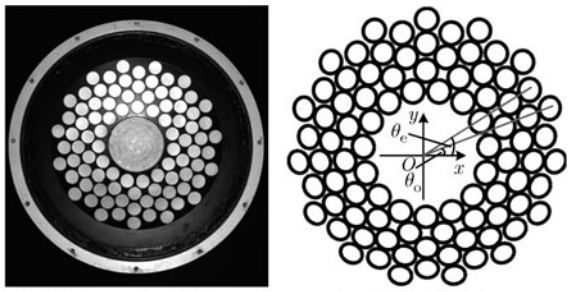

(a) Photograph of the array (b) Element distribution of the array

Fig. 1 A 90-element spherical phased array

The 90-element array (Shanghai Institute of Ceramics Chinese Academy of Sciences, Shanghai, China) was constructed with planar piezoelectric (PZT-8) elements and a spherical shell. The elements, which were distributed in six concentric rings, were mounted in the discrete concavities from the spherical shell with an 18 cm radius of curvature and a 21 cm diameter. Adhesives were then used to glue the elements and the concavities. To place the ultrasonic imaging transducer in the future development, a 5 cm central hole was placed in the spherical shell. Although the array geometry was said to be spherically sectioned, each element (1.4 cm in diameter and 0.2 cm thick) was tangent to the spherical shell surface at its center. The matching layers were affixed to the elements with the adhesives poured onto the external surface of the elements. Each element, which was electronically matched to 50 Ω using LC circuit, had its individual independent exciting unit in the ultrasound driving system. The voltage magnitude and phase of each element could thus be controlled independently. On the back of the array, one end of each copper wire, whose outside insulator was stripped, was soldered directly to each element electrode. The other end was installed on the back of the distributed printed circuit board (PCB). Afterwards, 90 square connectors were placed in front of the PCB, as such, each element was indirectly connected to a 5 m, SJ1563-80 coaxial cable. To avoid cross-talk between elements, 90 coaxial cables were then connected to the ultrasound driving system through a fixed 90-position socket connector panel. The ultrasound driving system could consume an electric power of up to about 1.4 kW, while the acoustic power

contributed by each element was about 6 W.

1.2 Simulations

The ultrasound field of a multiple-element phased array can be calculated through the superposition of the field generated by each element in the array. Each element should be divided into sufficient tiny areas such that the individual area can approximate to a point source. The ultrasound field from single element is therefore obtained by discretizations of the Rayleigh-Sommerfeld integral over these finite approximate point sources. In a homogeneous medium, for an array with N elements, the pressure p at an arbitrary point (x, y, z) is given by

$$p(x,y,z) = \mathrm{j}\frac{\rho c k}{2\pi}\sum_{n=1}^{N} v_n \sum_{\text{Surface}} \frac{A_n \mathrm{e}^{-(\alpha+\mathrm{j}k)r_n}}{r_n}, \qquad (1)$$

where, ρ is the density of medium ($1.0\times10^6\,\mathrm{kg/m^3}$); c is the speed of sound (1.5 km/s); k is the wave number, $k = 2\pi\nu/c$, ν is the resonance frequency (1 MHz); α is the attenuation coefficient; A_n is the corresponding divided area on the nth element; r_n is the distance between (x, y, z) and the divided point source on the nth element; and v_n represents the nth element's surface velocity as a function of amplitude and phase.

In this study, the ultrasound propagates in water and muscle one after another (see Fig. 2). The above principle can be also applied to a two-layer (water-muscle) medium. Assuming that the effect at the interface (reflection and refraction) can be ignored, which is largely true at the interface of water and muscle, if in addition the medium is homogeneous in both water and muscle layers, we have

$$p(x,y,z) = \mathrm{j}\frac{\rho c k}{2\pi}\sum_{n=1}^{N} v_n \times \sum_{\text{Surface}} \frac{A_n \mathrm{e}^{-(\alpha_\mathrm{w} r_n^\mathrm{w}+\alpha_\mathrm{m} r_n^\mathrm{m}+\mathrm{j}k r_n)}}{r_n}, \qquad (2)$$

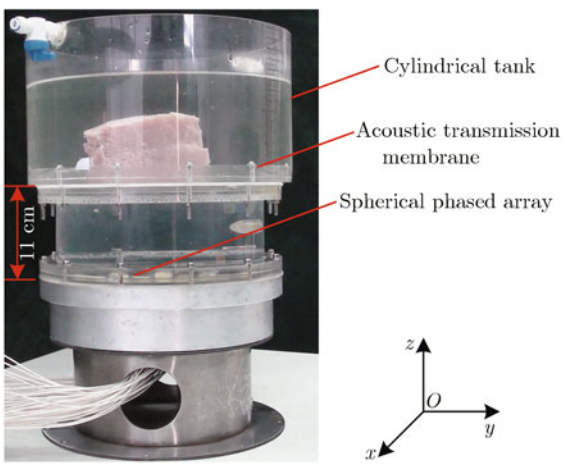

Fig. 2 A photograph of the experimental set-up

where, α_w and α_m are the attenuation coefficients in water and muscle ($\alpha_\mathrm{w} = 0$ and $\alpha_\mathrm{m} = 9\ \mathrm{Np/(m\cdot MHz)}$), respectively; r_n^w and r_n^m are the corresponding segments of r_n in medium water and muscle, respectively. The acoustic intensity I at the corresponding point (x, y, z) in the field can be obtained as follows,

$$I(x,y,z) = \frac{|p(x,y,z)|^2}{2\rho c}. \qquad (3)$$

The ultrasound fields of the proposed array focusing and steering at different depths were calculated to determine the effective focal depth. The quality of resulting intensity distributions in single focus mode is classified into four grades (A, B, C and D) according to the criteria proposed in Ref. [6]. The grade classification for intensity distributions is given as follows, I_max is the maximal value of I.

Grade A: $I \geqslant 0.1I_\mathrm{max}$, I occured only within the focal region;

Grade B: $0.1I_\mathrm{max} \leqslant I \leqslant 0.15I_\mathrm{max}$, outside the focal region there are less than 10 areas where I occured;

Grade C: $0.1I_\mathrm{max} \leqslant I \leqslant 0.15I_\mathrm{max}$, outside the focal region there are more than 10 areas where I occured;

Grade D: $I \geqslant 0.2I_\mathrm{max}$, I occured at least once outside the focal region.

In all calculations, the spatial resolution in the xOy plane was 0.25 mm, the spatial resolution along the z axis was also 0.25 mm, and the region of calculation was ±5 cm away from the focal plane along the z axis and ±2.5 cm from the z axis. All calculations were carried out using MATLAB V7.4.0 on a 2.53 GHz Celeron IV and 512 MB RAM-based PC.

1.3 Ex Vivo Experiments

The 90-element phased array was installed at the bottom of a polymethyl cylindrical tank. The tank, 22 cm in height and 24 cm in diameter, was filled with degassed and deionized water. Fresh excised porcine muscles obtained from butcher shops were cut into cubic units. These units were then laid on a clean plate until they reached the room temperature. The units were placed on an acoustic transmission membrane, which is 11 cm away from the array along the z axis (see Fig. 2).

Tests of ablating deep tissue with single focus mode were performed on muscle units. The focus positions were located in the $z = 15$ cm and $z = 19$ cm planes, which respectively mean 4 cm and 8 cm deep in units. The phase distributions were determined using the pseudo inverse method[5]. The elements had uniform voltage magnitudes. Following the sonications, the units were sliced first through the focal plane parallel to the xOy plane, and then sliced through the plane parallel to the xOz plane. The lesions were measured and photographed.

2 Results and Discussion

Figure 3 shows intensity distributions for the developed array in the single focus mode. The focus is displaced from 7 to 12 mm off the z axis (in the $z = 18$ cm plane), leading to the quality changed from Grade A to Grade D. In Fig. 3, there are four contours ($0.10I_{\max}$ to $0.25I_{\max}$ in increments of $0.05I_{\max}$) to determine the quality of the intensity distributions. Summarization about the grades for the quality of the intensity distributions associated with two different depths of water layers is demonstrated in Fig. 4. Figure 4 presents data for the focus shifted along the positive x axis. The above intensity distributions were obtained according to Eqs. (2) and (3), and the depth of water layer h was 11 cm in Fig. 4(a). Figure 4(b) illustrates the effect of reducing h. The quality of the intensity distributions shown in Fig. 4(b) is for another case when $h = 8$ cm.

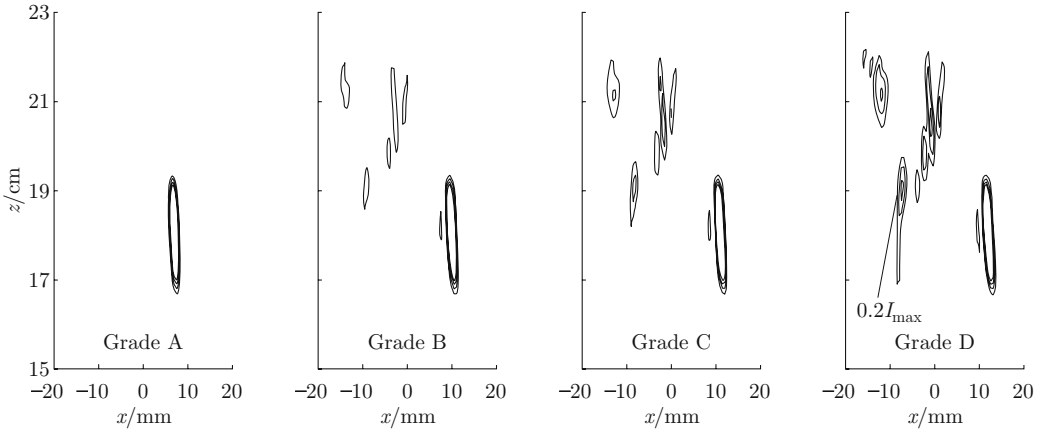

(a) (7, 0, 180) mm (b) (10, 0, 180) mm (c) (11, 0, 180) mm (d) (12, 0, 180) mm

Fig. 3 Grade classification for the quality of the intensity distributions and normalized intensity contours

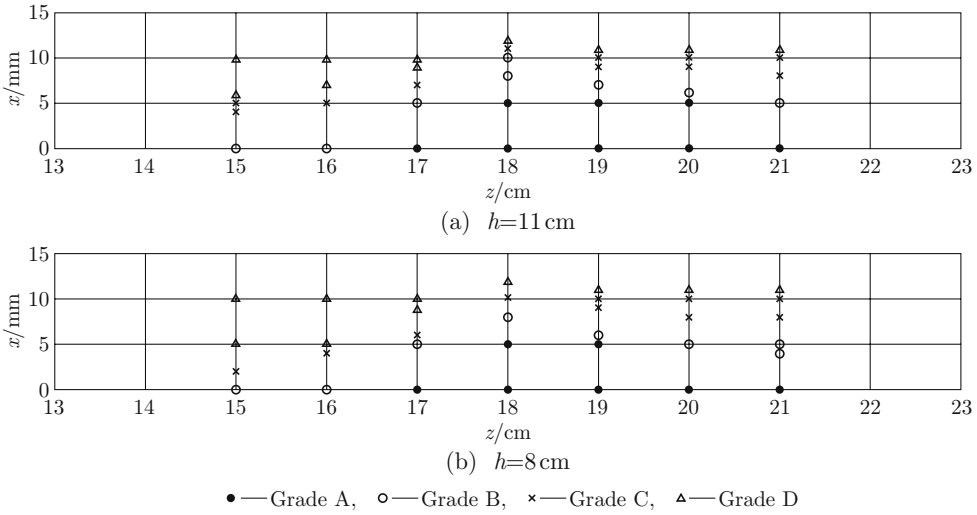

Fig. 4 Results of quality rates of the intensity distributions for the single focus modes generated by the developed array

Single focus modes at two different depths (15 and 19 cm) were synthesized in ex vivo experiments. And in each focal mode, the electric power consumed by the ultrasound driving system was about 700 W (half of the maximal power). Figure 5 shows one sample of the resulting lesions caused by the sonication focus at (0, 0, 15) cm for 20 s. The lesion shown in Fig. 6 was created at the focus at (0, 0, 19) cm for 60 s. Two parameters are used to evaluate the size of the cigar-shaped lesions: one parameter is the diameter of the circle which covers the lesions in the focal plane (xOy plane), while the other one is the height that is the length of the lesions in the z axis. The depth with the widest segment is chosen as the depth of the lesion from the unit surface, which is used to describe the practical depth of the heated region. Table 1 summarizes the data of the resulting lesions.

Overall the 90-element array demonstrated both in simulations and ex vivo experiments the ability of deep tissue ablation. The effective steering range of the developed array for single focus modes is determined by the quality of the intensity distributions that result

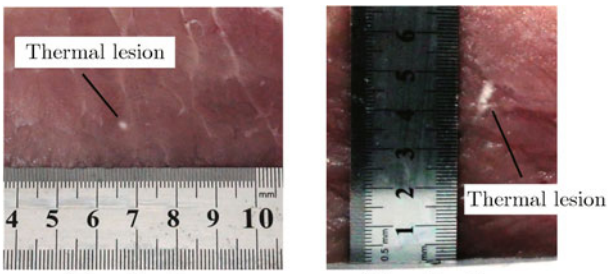

(a) xOy plane (b) xOz plane

Fig. 5 Thermal lesion produced by the focus at (0, 0, 15) cm for 20 s

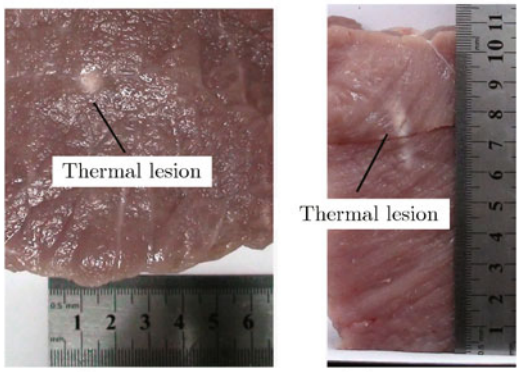

(a) xOy plane (b) xOz plane

Fig. 6 Thermal lesion produced by the focus at (0, 0, 19) cm for 60 s

Table 1 Summary of thermal lesions at two depths in single focus mode

	No.	Heating duration/ s	Lesion depth from surface/ mm	Lesion diameter/ mm	Lesion height/ mm
Focused at (0,0,15) cm	1	25	35	7	16
	2	25	37	4	15
	3	25	38	4	13
	4	22	38	3	10
	5	20	–	6	13
	6	20	45	3	10
	7	18	–	3	7
Focused at (0,0,19) cm	8	65	78	10	26
	9	60	75	10	22
	10	60	75	7	18
	11	60	78	7	17
	12	60	76	10	16
	13	50	no lesion	–	–
	14	50	no lesion	–	–
	15	50	no lesion	–	–

from the focus displacement of up to 15 mm off center over ranges from 15 to 21 cm. With the water depth at 11 cm, the developed array could shift the single focus up to 6 mm off center over ranges from 17 to 21 cm, which leads to a good quality (Grade A or B) (see Fig. 4(a)). As the water depth decreased to 8 cm, the intensity distributions with a good quality have changed little in the focus steering range (see Fig. 4(b)). Therefore, the developed array can ablate deep-seated tissue through the water depth adjustment. The lesions at about 4 and 8 cm deep from the surface were created within the muscle units using single focus modes (see Figs. 5 and 6). The heating duration to produce lesions depends on the target depth (see Table 1). Driven by the same electric power, heating duration is required to increase for the deeper target.

The depth of 8—12 cm from the organ surface is suitable for an extracorporeal treatments of most of the deep-seated organs (i.e., liver) in the thoracic and abdominal cavity[10]. To achieve the above ablation depth (8—12 cm) using the developed array, the water depth should be adjusted to 7—11 cm (taking 19 cm as the target focal depth). One of the problems that arise when ablating deep tissue is that the absorbed ultrasonic energy over the long focal distance might result in the necrosis along the propagation path. The experimental results are encouraging in that the lesions were generated only within the focal region while there was no discoloration area along the beam path.

The depths of the produced lesions from the surface are mostly less than 5 mm shorter than the target depths (4 or 8 cm, see Table 1), which is consistent with previous results. This phenomenon, which is identified as the displacement of the "biological" focal region, may cause the heated region misalignment with the desired target area.

To date, linear propagation models have been used in most models to calculate the intensity fields required to compute the temporally varying temperature distributions used to compute the thermal dose contours. In this study, the linear model was also used to calculate the pressure at an arbitrary point through the superposition of the pressure produced by each element of the array. Under some circumstances, the linear model has some limitations. Linear propagation of a focused wave in a uniformly absorbing medium will result in maximal energy deposition within the focal region. As the speed of sound increases with increasing pressure (i.e., the pressure maximum travels faster than the pressure minimum), the wavefront distorts as it propagates with increasing intensity, leading to a sawtooth waveform normally described as nonlinear propagation. Several parameters, an increase in any of which results in an enhancement of the nonlinear effect, include intensity (or pressure), propagation distance, viscosity and density of the medium and frequency. The acoustic nonlinearity will result in additional higher harmonics transferred from some of the energy of the initial fundamental frequency wave. These harmonics increase the

frequency-dependent absorption of ultrasound energy in soft tissue and even contribute to the lesion formation with the presence of sufficient intensity. Taking intensity and frequency into account, the ultrasound energy absorbed in the pre-focal region predicted by nonlinear propagation is many times greater than that predicted by linear propagation. Therefore, the nonlinear effect may account for the shift of the "biological" focal region, and in experiments it is observed in photos that the depth of the lesion from the surface does not coincide with the predetermined focus. How to relieve or even avoid the effect of this phenomenon should be reconsidered in the future study.

Given that spherical-section phased arrays have been confirmed to achieve good results in deep tissue ablation, many spherical phased arrays with various parameters (i.e., the shape, size, and distribution of elements) have been designed. Most of them[7] used the compact polygon distributions with the square elements. However circular elements distributed randomly or annularly can be another option in the spherical array designs. Previous studies[6] indicate that the array with random distribution of circular elements has a good performance in suppressing the grating lobes. In addition, random distributions offer a larger focus steering range with a good quality of intensity distributions in comparison with regular distributions. Nonetheless, random distributions require the element size not to exceed five sound waves, or else its advantages are insignificant. Considering the element size and practical fabrication level, the annular distribution may be a suboptimal choice for circular elements, and it has quite similar performance with the random arrays except higher grating lobes in the near field. The proposed array distributes the same number of circular elements in each concentric ring, which differs from those annular distributions in Ref. [6]. Such element distribution in the proposed array offers a design that allows a relatively small number of elements in the large array for deep tissue ablation.

Lastly, the ex vivo experiments on porcine muscles also demonstrated that a well-engineered phased array applicator could form lesions at a predetermined depth in tissue. The lesions were produced at about 4 and 8 cm deep from the muscle surface. The depth of 8 cm is suitable for almost all extremity treatments (i.e., breast tumor treatments and kidney treatments), and it would also be enough for some liver mass treatments.

3 Conclusion

This study has demonstrated that a 90-element spherical phased array using the annular distributions of circular elements can create lesions in deep tissue. The same number of elements distributed in each ring provides a relatively small number of elements but larger scale geometry in comparison with some other spherical arrays[7-9] for deep tissue ablation. The phased array can adjust the water depth to ablate the deep-seated tissue at various depths. Simulation results have illustrated that the phased array offers an effective focus steering range of up to 6 mm off center over ranges from 17 to 21 cm in the z axis when the water depth set at 11 cm. In addition, the water depth variance could yield little change in the focus steering range with good quality (Grade A or B). The ex vivo experiments also confirm the ability of the developed array to coagulate the tissue at depths of 4 and 8 cm. This study suggests that similar "low cost" arrays are effective and suitable phased arrays for creating lesions in deep tissue.

References

[1] Haar G T, Coussios C. High intensity focused ultrasound: Past, present and future [J]. *International Journal of Hyperthermia*, 2007, **23**(2): 85-87.

[2] Ebbini E S, Cain C A. A spherical-section ultrasound phased array applicator for deep localized hyperthermia [J]. *IEEE Transactions on Biomedical Engineering*, 1991, **38**(7): 634-643.

[3] Daum D R, Hynynen K. Theoretical design of a spherically sectioned phased array for ultrasound surgery of the liver [J]. *European Journal of Ultrasound*, 1999, **9**(1): 61-69.

[4] Hand J W, Shaw A, Sadhoo N, et al. A random phased array device for delivery of high intensity focused ultrasound [J]. *Physics in Medicine and Biology*, 2009, **54**(19): 5675-5693.

[5] Ebbini E S, Cain C A. Multiple-focus ultrasound phased-array pattern synthesis: Optimal driving-signal distributions for hyperthermia [J]. *IEEE Transactions on Ultrasonics, Ferroelectrics, and Frequency Control*, 1999, **36**(5):540-548.

[6] Gavrilov L R, Hand J W. A theoretical assessment of the relative performance of spherical phased arrays for ultrasound surgery [J]. *IEEE Transactions on Ultrasonics, Ferroelectrics, and Frequency Control*, 2000, **47**(1): 125-139.

[7] Lu M, Wan M, Xu F, et al. Design and experiment of 256-element ultrasound phased array for noninvasive focused ultrasound surgery [J]. *Ultrasonics*, 2006, **44**(Sup.): e325-e330.

[8] Zhang C, Chen Y. Investigation of a spherical-section ultrasound phased array for hepatic ablation [J]. *Journal of Zhejiang University: Science A*, 2007, **8**(8): 1237-1245.

[9] Ndjin W A, Melodelima D, Parmentier H, et al. Utility of a tumor-mimic model for the evaluation of the accuracy of HIFU treatment: Results of in vitro experiments in the liver [J]. *Ultrasound in Medicine and Biology*, 2008, **34**(12): 1934-1943.

[10] Damianou C, Hynynen K. Near-field heating during pulsed high temperature ultrasound hyperthermia treatment [J]. *Ultrasound in Medicine and Biology*, 1993, **19**(9): 777-787.